Sensors and Actuators B 268 (2018) 319–327

Contents lists available at ScienceDirect

Sensors and Actuators B: Chemical

journal homepage: www.elsevier.com/locate/snb

Fabrication of tungsten oxide nanofibers via electrospinning for gasochromic hydrogen detection

Fatemeh Tavakoli Foroushani [a], Hossein Tavanai [b,c,d,*], Mehdi Ranjbar [c,d,e], Hajir Bahrami [a]

[a] Department of Textile Engineering, Amirkabir University of Technology, Tehran, 84156-83111, Iran
[b] Department of Textile Engineering, Isfahan University of Technology, Isfahan 84156-83111, Iran
[c] Centre of Excellence in Applied Nanotechnology, Isfahan University of Technology, Isfahan 84156-83111,Iran
[d] Nanotechnology and Advanced Materials Institute, Isfahan University of Technology, Isfahan 84156-83111 Iran
[e] Department of Physics, Isfahan University of Technology, Isfahan 84156-83111, Iran

ARTICLE INFO

Article history:
Received 16 December 2017
Received in revised form 17 April 2018
Accepted 21 April 2018
Available online 22 April 2018

Keywords:
Tungsten oxide nanofibers
Electrospinning
Hydrogen gas sensor
Gasochromic effect

ABSTRACT

The application of tungsten oxide nanofibers for gasochromic hydrogen sensing is reported. Three tungsten oxide nanofibrous webs were fabricated by electrospinning proxopolyltungestic acid incorporated in polyvinylpyrrolidone. The samples were then calcinated to remove Polyvinylpyrrolidone to obtain tungsten oxide nanofibers. The tungsten oxide nanofiber samples had a grain form with an average fiber diameter of 103 nm, 181 nm and 293 nm. The tungsten oxide nanofibrous webs showed a very good sensitivity to concentartions of hydrogen (in argon) as low as 2% at room temperature. This is very important as the electrical hydrogen gas sensors need high temperatures to sense hydrogen. Upon contacting hydrogen, the almost colorless nanofibers turn into blue in less than 2 min. Cyclic hydrogen – oxygen exposure showed that the samples could be reused after two cycles. XRD, Raman and FTIR analysis showed a monoclinic crystalline structure for tungsten oxide (WO_3). After exposure to hydrogen which resulted in the formation of tungsten oxide bronze ($H_{0.23}WO_3$), the original monoclinic structure changed to tetragonal. After the removal of hydrogen and exposure to air, the samples gain back the monoclinic structure. XPS analysis revealed that the presence of a low amount of palladium chemical phase is sufficient for active sites of WO_3 to continue sensing hydrogen gas.

1. Introduction

Hydrogen gas which is one the most widely used gases in petrochemical, electronic and metallurgy industries, is considered as a renewable energy source. In spite of fossil based fuels, hydrogen is a clean fuel and there is no pollution involved when burning it. Thanks to its very low density, hydrogen has also found importance in applications like aerospace where keeping weight down is of paramount importance [1]. Hydrogen which is colorless, tasteless and odorless with very low ignition energy of 0.02 mJ, inflames in air very easily with concentration in the range of 4–75%. For this reason, detection of hydrogen by a proper sensor and preventing the threat of fire when using it is essential [1]. Up to present time, a range of sensors, namely field effect transistor (FET) [2], Schottky diode [3] , optical fiber [4], thermoelectric [5], surface acoustic wave [6] and semiconducting metal oxides [7,8] have been employed to detect hydrogen. Among these, semiconducting metal oxide based sensors have been studied more than others due to merits such as small size, easy fabrication, low cost, quick response and high sensitivity [9]. It is worth mentioning that the gas-sensing behavior of semiconductor sensors depends directly on their preparation methods and conditions [7].

Tungsten oxide is one of the most widely used metal oxides for hydrogen detection. It can detect hydrogen either by changing color [10] or changing electrical resistance [8]. Changing color is known as gasochromic [11]. Tungsten oxide has been employed in a variety of shapes like, film, nanorods and nanofibers as a hydrogen sensor [8,10,12] Generally, electrical based sensors have the major disadvantage of producing sparks and hence the threat of inflammation or even explosion of hydrogen. For this reason, application of electric sensor requires extra care and precaution. On the other hand, tungsten oxide is a much safer material to be employed as a sensor.

* Corresponding author at: Department of Textile Engineering, Isfahan University of Technology, Isfahan 84156-83111, Iran.
E-mail address: tavanai@cc.iut.ac.ir (H. Tavanai).

https://doi.org/10.1016/j.snb.2018.04.120
0925-4005/

Table 1
Characteristics and application of electrospun tungsten oxide nanofibers.

Tungsten precursor	Additive polymer	Nanofiber diameter (nm)	Analyte	Calcination conditions	Sensor type	Ref.
Tungsten powder	PVP[1]	100–500	–	500 °C–2 h	–	[35]
Tungsten wire	PVP	150	H_2	500 °C–1 h	Electrical resistance	[8]
Tungsten chloride	PMMA[2]	150–200	NO_2, CO	300 °C–8 h	Electrical resistance	[29]
Tungsten chloride	PVP	200	NH_3	300,450,600 °C–2, 5 h	Electrical resistance	[30]
Tungsten chloride	PVP	285	Acetone H_2S	500 °C–3 h	Electrical resistance	[31]
Tungstic acid	PVP	40	NH_3	500 °C–3 h	Electrical resistance	[32]
Tungstic acid	PVP	Wall thickness 300–500	Acetone	500 °C–1 h	Electrical resistance	[9]
Tungstic acid	PVP	100,130	Ethanol vapor	400,450,500,550 °C–1, 2 h	Electrical resistance	[33]
AMT powder	PVP	275	Acetone	450 °C–2 h	Electrical resistance	[34]

[1] Poly vinylpyrrolidone.
[2] Poly (methyl methacrylate).

It is the aim of this research to investigate fabrication of tungsten oxide nanofibers via electrospinning for gasochromic hydrogen detection. Literature review shows that up to now tungsten oxide sensors have been used mostly in the form of crystalline or amorphous layers, which have been fabricated through techniques such as sputtering [11,13], thermal evaporation [14], sol-gel dip-coating [15,16] and sol–gel spin coating [17]. However, some researches have also employed tungsten oxide in the form of colloidal nanoparticles [18] as well as nanowires [6,9] for detection applications. It has been reported that other metal oxides like molybdenum oxide [19] and vanadium oxide[20], some blended metals like magnesium–Y and magnesium–zirconium–nickel [21,22] as well as conducting polymers like polystyrene sulfonate – polyaniline [23] show gasochromic capacity.

The mechanism of gasochromic property of tungsten oxide is not yet well known, in spite of the fact that some researchers like George et al. [11] and Lee et al. [14] have put forward some models. These models have been accepted by some researchers and rejected by others [15,17,24,25]. However, research has shown that a quick gasochromic response requires applying a catalyst like platinum or palladium on the surface of the sensor [26]. In this context, catalyst has the role of speeding up the dissociation of hydrogen molecules to hydrogen atoms or ions and as a result, faster diffusion (spillover) inside the sensor material which leads to change of color [27]. Gasochromic tungsten oxide layers have also been employed in applications like smart windows, industrial monitors, transparency controllable car windows, solar cell panels, memory devices and optical switches [25].

High specific surface of nanofibers is considered as a merit for sensor applications [28]. Electrospinning is the most common technique employed for fabricating nanofibers. This technique has a good control over the uniformity of the fabricated nanofibers. As far as the literature review on tungsten oxide nanofibers is concerned, the first published paper dates back to 2006 by Lu et al. [29] who electrospun tungsten powder (as precursor)-poly vinylpyrrolidone (PVP) suspension, followed by calcination at 500 °C for 2 h to remove PVP and obtain tungsten oxide nanofibers. The diameter of tungsten nanofibers fabricated by Lu et al. is reported to be in the range of 100 nm–500 nm. In this case the photo luminescence of nanofibers was studied. The following research which involved fabrication of tungsten oxide/PVP nanofibers via electrospinning suspensions of tungsten oxide precursor/PVP followed by calcination of PVP to reach tungsten oxide nanofibers is summarized in Table 1 [8,9,29–35].

It must be pointed out that all the tungsten oxide nanofibers mentioned in Table 1 have been tested as gas sensor based on their electrical resistivity and not gasochromic. Moreover, the optimal sensor performance is reported to need temperatures in the range of 300 °C–500 °C. The novelty of the present work is in fact investigating the gasochromic characteristics of tungsten oxide nanofibers as hydrogen gas sensor in room temperature.

Table 2
Formulation of the three electrospinning solutions coded as 1, 2 and 3.

Sample	PVP MW (kDa)	PPTA/Ethanol(v/v)	PVP/(Ethanol+PPTA) (g/ml)
1	29	0.6/3	0.27
2	1300	1.8/1.8	0.06
3	29	2.1/1.4	0.18

2. Material and methods

2.1. Synthesis of proxopolytungstic acid (PPTA)

PPTA is a common tungsten precursor which has been synthesized by Kudo [36]. In this work PPTA was synthesized according to Kudo as follows. Pure tungsten wire was fist cut to small pieces and then washed with soap, acetone, ethanol, followed by ultrasonic bath and finally rinsing with deionized water. In the next stage, 20 ml of hydrogen peroxide (30%, Merck) was added to 5 g of dried pieces of tungsten and left to gradually dissolve in dark at room temperature for 72 h. After complete dissolution, a platinum wire was positioned in the solution for 1 h to remove all the remaining hydrogen peroxide by dissociating it into water and oxygen. After removing platinum wire from the sol, 20 ml of ethanol (80 °C, Merck) was added to the solution and left until the milky color of the solution changed to light yellow. The solution was then filtered and stored in refrigerator (2–4 °C). Dewatering the sol with ethanol was carried out for sample C only and had to be cancelled for samples A and B as the dewatered sol led to needle blockage.

2.2. Preparation of electrospinning solutions

Three electrospinning solutions were prepared by first mixing PPTA sol in ethanol and then gradually adding PVP (Sigma Aldrich) to it, followed by stirring at room temperature until a homogenous solution was obtained. The molecular weight of PVP, the ratio of PPTA/ethanol and the ratio of PVP to PPTA/ethanol are shown in Table 2.

2.3. Electrospinning

The electrospinning set up consisted of a dosing pump (TERUMO, STC-527 Japan) equipped with a 1 ml syringe with blunt point needle, a high voltage supply (Emersun, 220 V) and an aluminum foil covered rotating drum as collector which was connected to negative electrode of the power supply. The needle tip was connected to the positive electrode. The electrospinning of the prepared solutions was carried out for 10 h for each sample according to electrospinning conditions mentioned in Table 3. It must be pointed out that these conditions were found by trial and error experiments for the three samples to give beadles and rather uni-

Table 3
The electrospinning conditions for the three PPTA/PVP solutions.

Sample	Voltage (kV)	Feed rate (ml/h)	Nozzle–collector distance (cm)
1	19	0.3	16
2	17	0.4	16
3	20	0.8	16

form fibers. The nanofibers were collected on the rotating collector revolving at 100 rpm.

2.4. Calcination

Calcination of the electrospun PPTA/PVP nanofibrous web was carried out to remove the additive PVP and ascertain tungsten oxide nanofibers. A furnace (Exciton, EX.1200-2L) was employed for this purpose. Temperature was raised from room temperature to 500 °C with a rate of 5 °C per minute. Calcination was continued at 500 °C for 2 h.

2.5. Characterization

Scanning electron microscope (SEM (Philips, XL30)) and Field emission scanning electron microscope (FESEM) (Hitachi, S4160) were used to study the surface morphology of the electrospun nanofibers. FTIR (Hartmann & Braun, MB Series BOMEM) was employed to investigate any reaction or interaction occurring as a result of mixing PPTA with PVP.

Raman (FIRSTGUARD, RIGAKU (1064)) was also employed to complete the information gained by FTIR. XRD (Asenware, AW-XDM300) was used to study the microstructure of the electrospun nanofibers. XPS was performed in an ESCA/AES system (Model Thermo Scientific EXCALAB 250Xi) using a Mg X-ray source. The binding energies were calibrated using C1 s binding energy (284.8 eV).

2.6. Gasochromic test of tungsten oxide nanofibrous webs

To carry out the gasochromic test, 0.03 g of each sample was positioned on a microscope glass substrate and wetted with 0.1 ml of palladium chloride ($PdCl_2$) solution to activate the fibers. The $PdCl_2$ solution was prepared by adding 0.02 g of $PdCl_2$ powder (59%pd, Merck) to a mixture of 99.9 ml deionized water containing 0.1 ml HCl. The samples were then positioned on the flat stage of a homemade stainless steel gas chamber with inlet and outlet pipes as well as a top glass window which made filming and taking picture of the color change possible (Fig. 1). The chamber was fed with different concentrations of hydrogen in argon with a rate of 1 l/min for 6 min. Images were taken as shown in the corresponding Figs. After 6 min of hydrogen exposure, the chamber window was opened to let the air in, which led to the disappearance of the color of the samples. The samples were then tested in a cyclic hydrogen (10% in argon v/v) – oxygen exposure.

Fig. 1. Homemade Stainless steel gas chamber with gas inlet and outlet as well as a top glass window.

2.7. Color characterization

Reflectance spectrophotometer (Datacolor 600, Light source = D65) was employed for the objective assessment of the color of the samples exposed to hydrogen gas after 6 min. This objective assessment was carried out by measuring CIE L*a*b* and K/S. K/S is a measure of the depth of the color of the sample which can be calculated from Eq. (1).

$$\frac{\boldsymbol{K}}{\boldsymbol{S}} = \frac{(1-\boldsymbol{R})^2}{2\boldsymbol{R}} \quad (1)$$

Where R is the reflectance at the dominant wavelength. CIE L* shows the lightness of the color of the sample. The higher the lightness, usually the lower is the depth. CIE a* (positive) shows redness, CIE a*(negative) greenness, CIE b*(positive) yellowness and CIE b*(negative) blueness.

3. Results and discussion

3.1. Nanofiber characterization

The SEM micrographs of PPTA-PVP nanofibers before calcination (A, B. and C) and tungsten oxide nanofibers (D, E and F) (after calcination) are shown in Fig. 2. A and D refer to sample 1, B and E refer to sample 2 and C and F refer to sample 3. As can be seen all the three PPTA-PVP electrospun nanofibers are uniform and beadless. The average diameter of the nanofibers electrospun from sample 1, 2 and 3 is 199 nm (A), 205 nm (B), and 755 nm (C), respectively. The SEM micrographs of tungsten oxide nanofibers are shown as D, E and F (corresponding to A, B and C, respectively) in Fig. 2. As can be seen, after calcination, the diameter of nanofibers drops considerably from 199, 205, 755 nm to 103, 182 and 293 nm, respectively. SEM micrographs also show that contrary to PPTA/PVP nanofibers, tungsten oxide nanofibers don't show a flat surface and seem to be composed of particles attached to each other linearly. This structure is particularly pronounced for D and E samples. This surface morphology is obviously formed when the matrix of PVP leaves the system as a result of pyrolysis process. Hence it is concluded that nanofiber diameter reduction, which is depicted in Fig. 3, is a result of pyrolysis.

Fig. 4 shows the FTIR spectrum of PVP powder, PPTA-PVP nanofibers and tungsten oxide nanofibers. As can be seen, PVP shows its characteristic peaks at 3452 cm^{-1} (O—H from water), 2955 cm^{-1} (C—H, asymmetric stretching SP^3), 1663 cm^{-1} (C=O, amide), 1423 cm^{-1}(C—H bending of methylene groups), 1288 cm-1(C—N), 934 cm^{-1}(C—C), 734 cm^{-1}(C—C chain) 651 and 570 cm^{-1} (N—C=O, bending). These characteristic peaks have also been obtained by Koczkur et al. [37] and Basha [38]. The spectrum of PPTS-PVP (Fig. 4b) shows all the characteristic peaks of PVP as well as peaks at 976 cm^{-1} (W=O, stretching) and a number of peaks in the range of 820–610 cm^{-1} (W-O-W) which are characteristic for PPTA[15]. An extended version of the spectrums of PVP and PPTA in the range of 1200–400 cm^{-1} is shown in Fig. 5. These spectra are normalized with respect to the C—H peak (SP^3). As far as tungsten oxide nanofiber is concerned, as can be seen from its spectrum (Fig. 4c), only a rather wide peak at about 806 cm^{-1} is observed. Nanba et al. has also observed the same peak for tungsten oxide [39]. In fact, the absence of PVP characteristic peaks in tungsten oxide nanofibers show the almost complete removal of PVP as a matrix during calcination. The wide peak at 806 cm^{-1} (O—W—O, stretching) is considered as a sign of the formation of crystalline tungsten oxide from its precursor (PPTA). In order to gain more

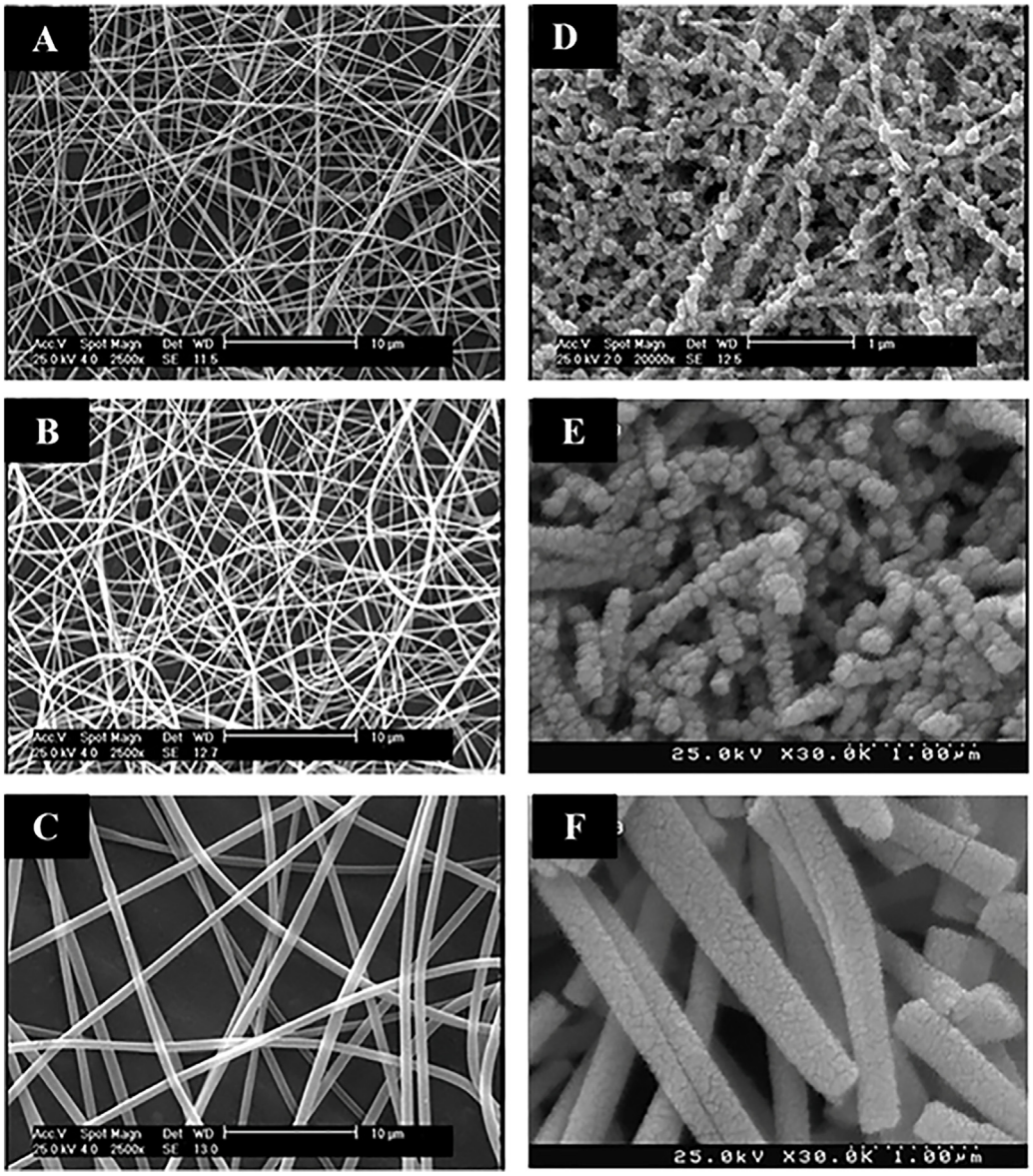

Fig. 2. SEM micrographs of PPTA-PVP nanofibers (A, B. and C before calcination) and tungsten oxide nanofibers (D, E and F after calcination), A and D from sample 1, B and E from sample 2, C and F from sample 3.

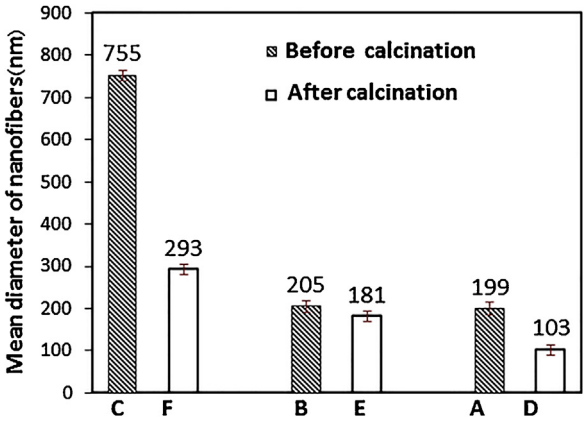

Fig. 3. Mean diameter of electrospun nanofibers before and after calcination.

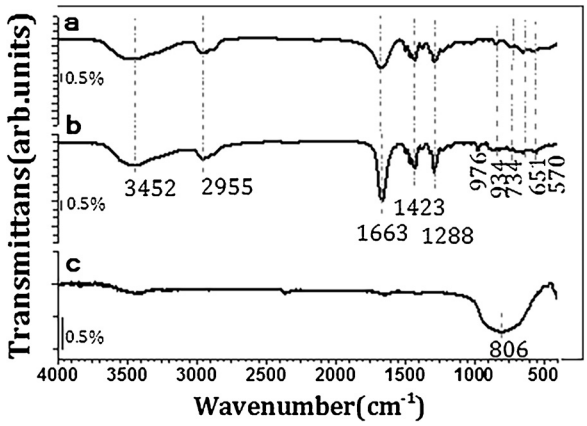

Fig. 4. FTIR spectrum of a) PVP, b) PPTA-PVP naofibers and c) Tungsten oxide nanofibers.

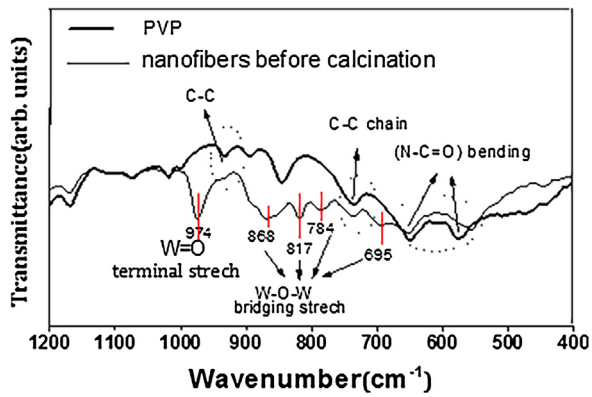

Fig. 5. Extended version of the spectrums of PVP and PPTA in the range of 1200–400 cm^{-1} normalized with respect to the C—H peak (SP^3).

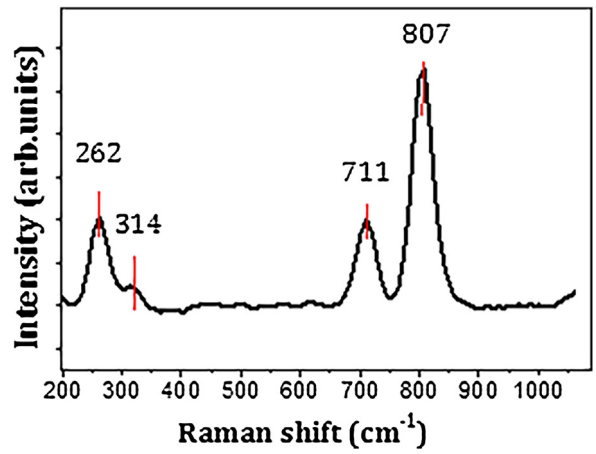

Fig. 6. Raman spectrum of tungsten oxide nanofibers (sample 2).

information on the physical and chemical structure of tungsten oxide nanofibers, Raman analysis was carried out as well which is shown in Fig. 6. The Raman shifts at 807 and 711 cm^{-1} originate from the symmetric and asymmetric stretching O—W—O, and the ones at 262 and 314 cm^{-1} are related to bending of W-O-W. It is worth saying that hereby, the monoclinic crystalline phase of tungsten oxide nanofibers is also verified.

XPS was employed for the sample 2 after adding a drop of $PdCl_2$ to the sample. The XPS results are shown in Fig. 7. The peaks at (35.7–37.7 eV), (284.8 eV) and (530–532 eV) show the presence of Tungsten, carbon and oxygen, respectively. Moreover, the small peaks at (330–345 eV) and (195–205 eV) indicate the presence of palladium and chlorine. The peak of W spectrum can be deconvoluted into four peaks. The strong doublet located at 35.6 and 37.7 eV are related to $W_{4f7/2}$ and $W_{4f5/2}$ core level transitions, respectively indicating the presence of W^{6+} (W^{VI}) in WO_3 structure [18]. The small doublet at 37.0 and 34.5 eV is attributed to W^{5+}(W^{V}). This probably indicates that a very small portion of surface chemical states consist of some oxygen defects that may act as nucleation sites for the spontaneous reduction of Pd ions. O_{1S} peak can be deconvoluted into two main peaks; one centered at 530.4 eV and a broad intense peak at 532.6 eV [18]. The first one is related to oxygen bonding with tungsten atoms while the next one is due to the

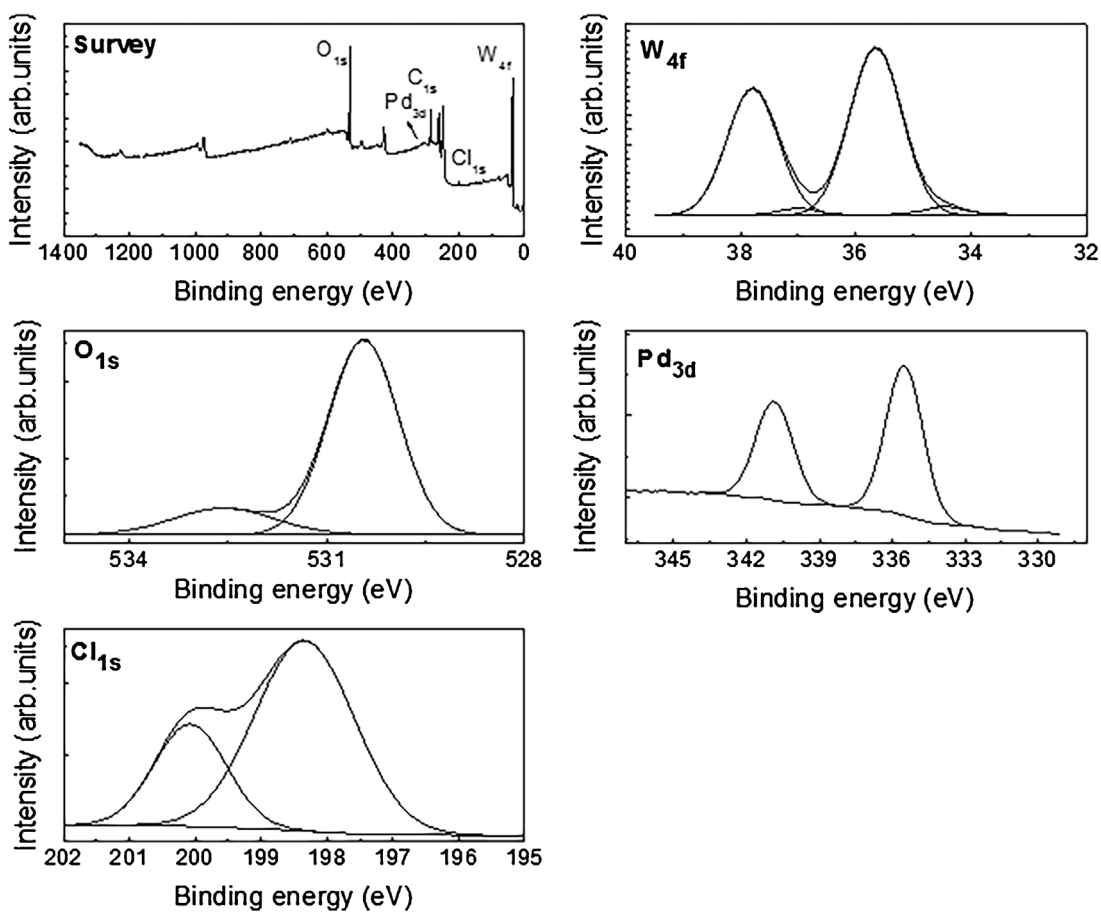

Fig. 7. XPS analysis of the tungsten oxide nanofibrous web wetted with palladium chloride.

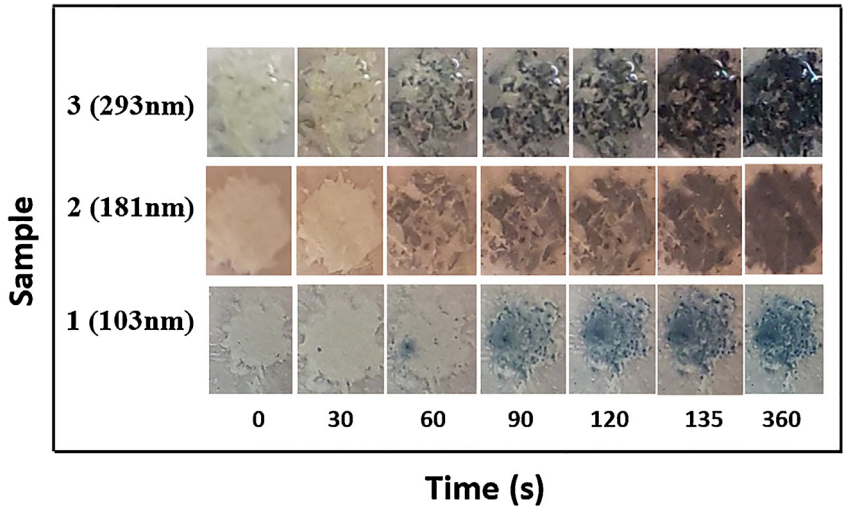

Fig. 8. Change of color of nanofibrous tungsten oxide web in hydrogen – argon (10–90) gas with time.

Table 4
L*a* b* of the nanofibrous tungsten oxide webs immediately after removal from the gas chamber containing hydrogen- argon (10- 90) (exposure time = 25 min).

sample	L*	a*	b*
1 (103 nm)	39.4	−7.5	−14.6
2 (182 nm)	34.3	−0.5	−11.6
3 (293 nm)	29.46	1.5	−11

presence of O—H, O—C and/or oxygen contaminants absorbed from the atmosphere [18,40].

High resolution XPS spectra of Pd_{3d} is deconvoluted into $Pd_{3d5/2}$ and $Pd_{3d3/2}$ peaks doublet located at 335.5 and 340.9 eV, respectively which are consistent with those reported for Pd. Nevertheless, because the signal of Pd is very low, it is not possible to detail interpretation of palladium states. However, the peak positions of $Cl_{2p3/2}$ and $Cl_{2p1/2}$, centered at 198.3 and 200.1 eV [40], respectively indicate that the majority of surface states are related to $PdCl_2$ which can be reduced after hydrogen exposure.

It must be said that the presence of a low amount of palladium chemical phase is sufficient for active sites of WO_3 to continue sensing hydrogen gas. One can state that there are some W^{5+} surface states that can promote reduction of palladium. Palladium in the form of ionic states or metal are considered as active sites for the initiation of gasochromic process.

3.2. Gasochromic characterization

Fig. 8 shows the change of the color of nanofibrous tungsten oxide web in hydrogen–argon (10–90) gas with time up to 6 min. As can be seen the original pale yellow color of all the three sample changes to blue, in other words hydrogen is detectet in about 60–90 s. With longer exposure times, the depth of color intensifies to some extent and the blue parts cover more surface. Table 4 shows L*a* b* of the nanofibrous tungsten oxide webs immediately after removal from gas chamber containing hydrogen- argon (10–90) (exposure time = 25 min).

Fig. 9. Depicts the Spectrophotometer of tungsten oxide nanofibrous webs immediately after removal from gas chamber containing hydrogen- argon (10–90) (exposure time = 25 min). The background has been subtracted from the spectrogram of the samples. The higher reflection of sample 1 nanofibers is due to their higher surface area and higher surface reflection from the surface. As the calculated K/S (showing of the depth of color) shows, the color depth increases with increasing diameter of the nanofibers.

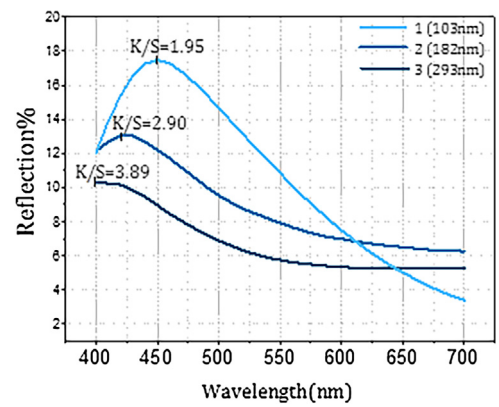

Fig. 9. Reflection versus of tungsten oxide nanofibrous webs.

However, although no substantial difference can be considered for the response time and response sensitivity of the samples, it maybe concluded that the lower diameter of nanofibers leads to a better contrast.

To test the applicability of the samples in low concentrations of hydrogen, experiments were carried out with low concentrations of 1, 2, 3 and 4% of hydrogen in argon. It is worth mentioning that as already stated, concentrations of higher than 4% of hydrogen are inflammable. In this part we chose sample 2 which had the highest share of WO_3 among the three samples. It was found that with these low concentrations, the amount of $PdCl_2$ catalyst used in the first stage of the work (high concentrations of hydrogen) was not enough; so the amount of catalyst had to doubled to 0.2 ml. The other conditions were the same as the previous experiments. It was found that sample 2 showed a very good sensitivity to hydrogen concentrations as low as 2%. This is shown in Fig. 10.

3.3. Microstructural characteristics

Fig. 11. depicts the XRD spectrum of tungsten oxide nanofibers (sample 2) before exposure to hydrogen- argon (10–90), immediately after removal from the gas chamber (exposure = 25 min) and 20 h after removal from the chamber (exposure = 25 min). The sharp peaks at 2θ = 23.1, 23.6, 24.2, 26.6, 28.8, 33.4, 33.8, 34° in Fig. 9a highlight the monoclinic crystalline phase of tungsten oxide (WO_3) with network parameters of a = 7.2970 Å b = 7.5390 Å c = 7.6880 Å and α, γ = 90° β = 90.91° (JCPDS Card No.00-043-1035). As already

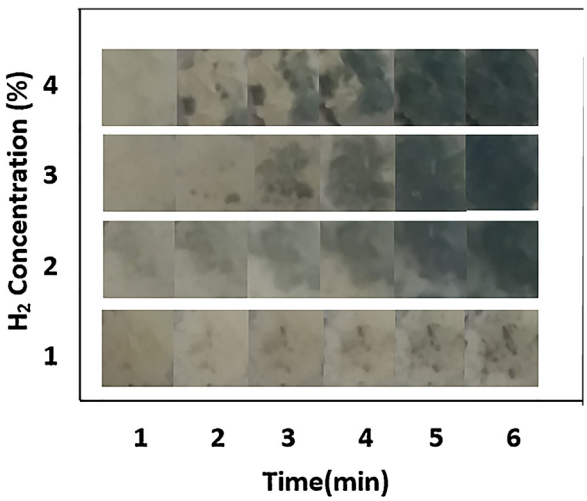

Fig. 10. The change of the color of nanofibrous tungsten oxide web (sample 2) in 1, 2, 3 and 4% hydrogen in argon.

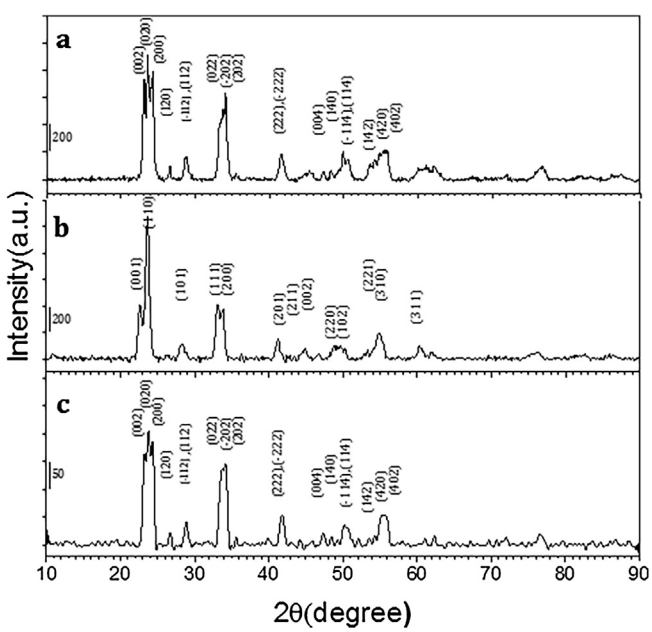

Fig. 11. XRD spectrum of tungsten oxide nanofibers a) before exposure to hydrogen-argon (10–90), b) immediately after removal from the gas chamber (exposure = 25 min) and c) 20 h after removal from the chamber (exposure = 25 min).

stated, this microstructural characteristic was also proved for tungsten oxide by the Raman spectra as well. However, after exposure to hydrogen gas (while the sample has its new color), the XRD spectrum (Fig. 9b) changes and the new spectrum shows sharp peaks at 2θ = 22.5, 23.6, 28.1, 33, 33.8° indicating tetragonal crystalline phase of hydrogen tungsten oxide ($H_{0.23}WO_3$) with network parameters of a = 5.2285 Å b = 5.2285 Å c = 2.8810 Å and α, β, γ = 90° (JCPDS Card No. 01-085-0967).

As the samples gradually lose the color with time after removal from the chamber, XRD analysis was also carried out for sample 2, 20 h after being removed from the chamber. At this stage the sample had recovered the original pale yellow color as shown in Fig. 9c. As can be seen the XRD spectrum of the sample before exposure is basically repeated for the sample after recovery. So it is concluded that as far as the microstructure is concerned, the original monoclinic microstructure is recovered after losing the color change which occurred as a result of exposure to hydrogen gas.

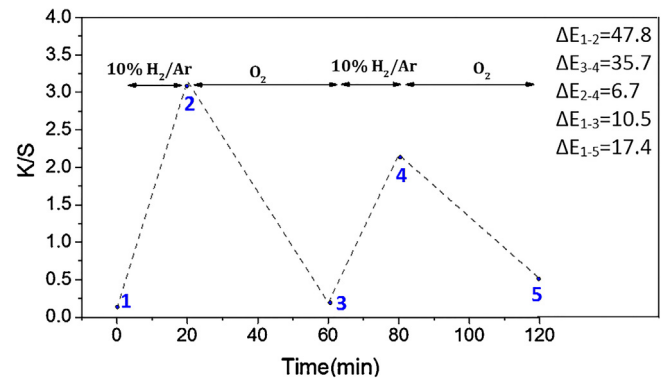

Fig. 12. K/S versus time as well as the color differences (Δ*E*) for sample 2 during 2 cyclic hydrogen- oxygen exposure.

Table 5
CIE L* a* b* for sample 2 at different stages of cyclic hydrogen – oxygen exposure (Fig. 12)

step	L*	a*	b*	K/S
1	81.83	−6.94	14.68	0.12
2	38.36	−1.26	−4.39	3.15
3	77.69	−6.02	5.01	0.19
4	43.25	−5.81	−4.27	2.17
5	66.74	−6.24	4.93	0.51

3.4. Color change after cyclic exposure to hydrogen and oxygen

The cyclic hydrogen oxygen exposure has been carried out for two cycles. CIE L*a*b* and K/S as well as the color differences (Δ*E*) have been shown in Fig. 12. and Table 5. It must be pointed out the samples could be utilized for hydrogen detection only up to two times. The color difference is calculated according to the Eq. (2). It is worth mentioning that color difference (Δ*E*) above 2.5–3 is usually visible to the naked eye.

$$\Delta E = \sqrt{\Delta l^{*2} + \Delta a^{*2} + \Delta b^{*2}} \quad (2)$$

3.5. Gasochromic mechanism

When hydrogen reaches $PdCl_2$ solution, palladium ions gradually begin to reduce to Pd, due to the interaction between hydrogen and $PdCl_2$. Then, H_2 is dissociated into two H^+ and two free electrons by Pd which acts as a catalyst. This process is known as spillover. The dissociated protons and electrons diffuse into the WO_3 lattice and occupy the available sites (double injection). As a result, tungsten oxide bronze ($H_xW^{VI}_{1-x}W^V_xO_3$) which is a mixture of W^{VI} and W^V forms. It is in fact the W^V which has the blue color. It is worth mentioning that WO_3 (W^{VI}) is pale yellow. The reaction mechanism can be written as follows.

$$\boldsymbol{H_2 \xrightarrow{Pd} 2H^+ + 2e^-}$$

$$\boldsymbol{2H^+ + 2e^- + WO_3 \rightarrow H_xW^{VI}_{1-x}W^V_xO_3}$$

The following schematic diagram shown in Fig. 13 represents the gasochromic mechanism.

4. Conclusions

Tungsten oxide nanofibers with an average diameter of 103 nm, 181 nm and 293 nm were successfully prepared. These colorless nanofibers were capable of detecting hydrogen gas with a concentration of as low as 2% in a matter of less than 2 min by turning into blue. A monoclinic crystallin structure was observed for tungsten

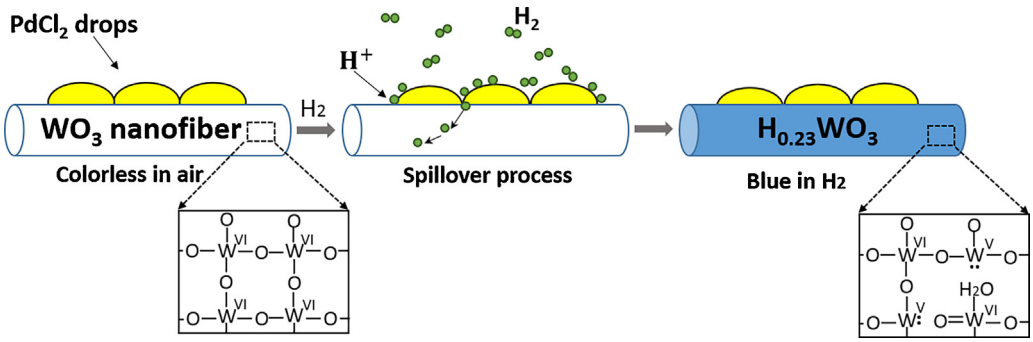

Fig. 13. Schematic representation of the gasochromic mechanism.

oxide (WO_3) with the help of XRD, Raman and FTIR analysis. The original monoclinic structure of tungsten oxide (WO_3) changed into tetragonal structure, after exposure to hydrogen which resulted in the formation of tungsten oxide bronze ($H_{0.23}WO_3$). After the color recovery upon air exposure, the monoclinic structure was recovered. Cyclic hydrogen – oxygen exposure showed that the samples enjoyed the capability of hydrogen detection for the second time. The presence of a low amount of palladium chemical phase is sufficient for active WO_3 sites to continue sensing hydrogen gas. This was shown by XPS analysis. Hydrogen gas sensors based on tungsten oxide nanofibers do not have the danger of producing sparks which can lead to explosion in certain conditions. Being capable of sensing hydrogen in room temperature is a major advantage of the tungsteun oxide nanofibrous sensors

Acknowledgements

The authors would like to express their sincere thanks and gratitude to Prof. Somaye Fardindoost and Eng. Amir Bagheri for their kind cooperation.

References

[1] A. Lanz, J. Heffel, C. Messer, Hydrogen Fuel Cell Engines and Related Technologies: College of the Desert, Energy Technology Training Center, 2001.
[2] T. Higuchi, S. Nakagomi, Y. Kokubun, Field effect hydrogen sensor device with simple structure based on GaN, Sens. Actuators B 140 (2009) 79–85.
[3] T.-H. Tsai, H.-I. Chen, K.-W. Lin, C.-W. Hung, C.-H. Hsu, L.-Y. Chen, et al., Comprehensive study on hydrogen sensing properties of a Pd–AlGaN-based Schottky diode, Int. J. Hydrogen Energy 33 (2008) 2986–2992.
[4] Y. Liu, Y. Li, Enhanced sensitivity of transmission based optical fiber hydrogen sensor with multi-layer Pd–Y alloy thin film, Sens. Actuators B 227 (2016) 178–184.
[5] M. Nishibori, W. Shin, N. Izu, T. Itoh, I. Matsubara, S. Yasuda, et al., Robust hydrogen detection system with a thermoelectric hydrogen sensor for hydrogen station application, Int. J. Hydrogen Energy 34 (2009) 2834–2841.
[6] W. Jakubik, Investigations of thin film structures of WO 3 and WO 3 with Pd for hydrogen detection in a surface acoustic wave sensor system, Thin Solid Films 515 (2007) 8345–8350.
[7] A. Adamyan, Z. Adamyan, V. Aroutiounian, A. Arakelyan, K. Touryan, J. Turner, Sol-gel derived thin-film semiconductor hydrogen gas sensor, Int. J. Hydrogen Energy 32 (2007) 4101–4108.
[8] A. Nikfarjam, S. Fardindoost, Fabrication of Pd doped WO3 nanofiber as hydrogen sensor, Polymers 5 (2013) 45–55.
[9] X. Bai, H. Ji, P. Gao, Y. Zhang, X. Sun, Morphology, phase structure and acetone sensitive properties of copper-doped tungsten oxide sensors, Sens. Actuators B 193 (2014) 100–106.
[10] S. Chen, J. Luo, H. Tan, J. Chen, S. Deng, N. Xu, Study of self-heating phenomenon and its resultant effect on ultrafast gasochromic coloration of Pt-WO 3 nanowire films, Sens. Actuators B 173 (2012) 824–832.
[11] A. Georg, W. Graf, R. Neumann, V. Wittwer, Mechanism of the gasochromic coloration of porous WO 3 films, Solid State Ionics 127 (2000) 319–328.
[12] M. Horprathum, T. Srichaiyaperk, B. Samransuksamer, A. Wisitsoraat, P. Eiamchai, S. Limwichean, et al., Ultrasensitive hydrogen sensor based on Pt-decorated WO3 nanorods prepared by glancing-angle dc magnetron sputtering, ACS Appl. Mater. Interfaces 6 (2014) 22051–22060.
[13] M. Stolze, B. Camin, F. Galbert, U. Reinholz, L. Thomas, Nature of substoichiometry in reactively DC-sputtered tungsten oxide thin films and its effect on the maximum obtainable colouration by gases, Thin Solid Films 409 (2002) 254–264.
[14] S.-H. Lee, H.M. Cheong, P. Liu, D. Smith, C.E. Tracy, A. Mascarenhas, et al., Raman spectroscopic studies of gasochromic a-WO 3 thin films, Electrochim. Acta 46 (2001) 1995–1999.
[15] B. Orel, N. Grošelj, U.O. Krašovec, R. Ješe, A. Georg, IR spectroscopic investigations of gasochromic and electrochromic sol-gel—derived peroxotungstic acid/ormosil composite and crystalline WO 3 films, J. Sol-Gel Sci. Technol. 24 (2002) 5–22.
[16] U. Opara-Krašovec, R. Ješe, B. Orel, J. Grdadolnik, G. Dražič, Structural, vibrational, and gasochromic properties of porous WO 3 films templated with a sol-gel organic–inorganic hybrid, Monatshefte für Chemie/Chemical Monthly 133 (2002) 1115–1133.
[17] C.-C. Chan, W.-C. Hsu, C.-C. Chang, C.-S. Hsu, Hydrogen incorporation in gasochromic coloration of sol–gel WO 3 thin films, Sens. Actuators B 157 (2011) 504–509.
[18] M. Ranjbar, A.H. Fini, H. Kalhori, P. Kameli, H. Salamati, Gasochromic effect in colloidal nanoparticles of tungsten oxide dihydrate synthesized via a simple anodizing method, Sol. Energy Mater. Sol. Cells 132 (2015) 329–336.
[19] F. Delalat, M. Ranjbar, H. Salamati, Blue colloidal nanoparticles of molybdenum oxide by simple anodizing method: decolorization by PdCl 2 and observation of in-liquid gasochromic coloration, Sol. Energy Mater. Sol. Cells 144 (2016) 165–172.
[20] M. Ashrafi, M. Ranjbar, H. Kalhori, H. Salamati, Pulsed laser deposition of Mo-VO thin films for chromogenic applications, Thin Solid Films 621 (2017) 220–228.
[21] Y. Yamada, S. Kitamura, M. Miura, K. Yoshimura, Improving the optical properties of switchable mirrors based on Mg–Y alloy using antireflection coatings, Sol. Energy Mater. Sol. Cells 141 (2015) 337–340.
[22] K. Tajima, Y. Yamada, K. Yoshimura, Switchable mirror glass with a Mg–Zr–Ni ternary alloy thin film, Sol. Energy Mater. Sol. Cells 126 (2014) 227–236.
[23] C.-W. Hu, Y. Yamada, K. Yoshimura, A new type of gasochromic material: conducting polymers with catalytic nanoparticles, Chem. Commun. 53 (2017) 3242–3245.
[24] U.O. Krašovec, B. Orel, A. Georg, V. Wittwer, The gasochromic properties of sol–gel WO 3 films with sputtered Pt catalyst, Sol. Energy 68 (2000) 541–551.
[25] J.Y. Luo, S.Z. Deng, Y.T. Tao, F.L. Zhao, L.F. Zhu, L. Gong, et al., Evidence of localized water molecules and their role in the gasochromic effect of WO3 nanowire films, J. Phys. Chem. C 113 (2009) 15877–15881.
[26] W.-C. Hsu, C.-C. Chan, C.-H. Peng, C.-C. Chang, Hydrogen sensing characteristics of an electrodeposited WO 3 thin film gasochromic sensor activated by Pt catalyst, Thin Solid Films 516 (2007) 407–411.
[27] M.A. Behbahani, M. Ranjbar, P. Kameli, H. Salamati, Hydrogen sensing by wet-gasochromic coloring of PdCl 2 (aq)/WO 3 and the role of hydrophilicity of tungsten oxide films, Sens. Actuators B 188 (2013) 127–136.
[28] G. Korotcenkoc, *Handbook of Gas Sensor Materials: Properties, Advantages, and Shortcomings* for Applications. Springer, New York, 2013. Volume 1: Conventional Approaches (442 p.) Volume 2: New Trends and Technologies (454 p.).
[29] X. Lu, X. Liu, W. Zhang, C. Wang, Y. Wei, Large-scale synthesis of tungsten oxide nanofibers by electrospinning, J. Colloid Interface Sci. 298 (2006) 996–999.
[30] S. Piperno, M. Passacantando, S. Santucci, L. Lozzi, S. La Rosa, WO 3 nanofibers for gas sensing applications, J. Appl. Phys. 101 (2007) 124504.
[31] J.-Y. Leng, X.-J. Xu, N. Lv, H.-T. Fan, T. Zhang, Synthesis and gas-sensing characteristics of WO 3 nanofibers via electrospinning, J. Colloid Interface Sci. 356 (2011) 54–57.
[32] J. Shin, S.-J. Choi, D.-Y. Youn, I.-D. Kim, Exhaled VOCs sensing properties of WO3 nanofibers functionalized by Pt and IrO2 nanoparticles for diagnosis of diabetes and halitosis, J. Electroceram. 29 (2012) 106–116.
[33] T.-A. Nguyen, S. Park, J.B. Kim, T.K. Kim, G.H. Seong, J. Choo, et al., Polycrystalline tungsten oxide nanofibers for gas-sensing applications, Sens. Actuators B 160 (2011) 549–554.

[34] T.-H. Fang, S.-H. Yang, Y.-J. Hsiao, D.-M. Lu, The manufacture and characteristics analysis of electrospun tungsten trioxide nanofibers, Smart Sci. 4 (2016) 22–27.
[35] S. Wei, G. Zhao, W. Du, Q. Tian, Synthesis and excellent acetone sensing properties of porous WO 3 nanofibers, Vacuum 124 (2016) 32–39.
[36] T. Kudo, H. Okamoto, K. Matsumoto, Y. Sasaki, Peroxopolytungstic acids synthesized by direct reaction of tungsten or tungsten carbide with hydrogen peroxide, Inorg. Chim. Acta 111 (1986) L27–L28.
[37] K.M. Koczkur, S. Mourdikoudis, L. Polavarapu, S.E. Skrabalak, Polyvinylpyrrolidone (PVP) in nanoparticle synthesis, Dalton Trans. 44 (2015) 17883–17905.
[38] M.A.-F. Basha, Magnetic and optical studies on polyvinylpyrrolidone thin films doped with rare earth metal salts, Polym. J. 42 (2010) 728.
[39] T. Nanba, S. Takano, I. Yasui, T. Kudo, Structural study of peroxopolytungstic acid prepared from metallic tungsten and hydrogen peroxide, J. Solid State Chem. 90 (1991) 47–53.
[40] M. Ranjbar, S. Fardindoost, S.A. Mahdavi, Palladium nanoparticle deposition onto the WO3 surface through hydrogen reduction of PdCl2: characterization and gasochromic properties, Sol. Energy Mater. Sol. Cells 95 (2011) 2335–2340.

Biography

Professor Hossein Tavanai PhD (Leeds), Hossein Tavanai is a member of faculty in the department of Textile Engineering of Isfahan University of Technology (Iran). He gained his B.SC (1980), M.SC (1981) and PhD (1995) From the University of Leeds. His PhD research which was carried out under the supervision of Dr. M.J. Denton and Dr. J.G. Tomka involved the structure and properties of low filament number false-twist draw-textured polyamide yarns. After gaining experience in Hoechst, Bayer, BASF and Ciba-Geigy, he joined the academic staff of the Department of Textile Engineering of Isfahan University of Technology in 1986 and has lectured on texturizing, cloth printing, dyeing techniques and fiber physics since then. A number of textile books in Farsi have been written by him. Hossein Tavanai has recently been very actively involved in research concentrating on the electrospraying of natural polymers, electrospinning and activated carbon nanofibers as well as nano composite nanofibers and conductive polymer coated nanofibers. He has spent one year at the center for material and fiber innovation (CMFI), Deakin University (Geelong, Victoria) as visiting Professor.